Combined Ferroelastic and Optical Control of Electronic Transport in Mott-Oxide–Ferroelectric Heterostructures

Ming Zheng,* Pengfei Guan, Xiang Ji, and Litong Guo
School of Materials Science and Physics, China University of Mining and Technology, Xuzhou 221116, China

(Received 15 September 2021; revised 9 November 2021; accepted 3 January 2022; published 24 January 2022; corrected 25 January 2023)

Diverse external stimuli, such as light irradiation, an electric field, and a stress field, are employed to trigger the large modulation of electronic properties in Mott insulators. Here, we demonstrate that multiple nonvolatile and reversible resistivity evolution can be realized by adjusting the magnitude of ferroelastic strain in voltage-actuated $LaVO_3/0.7Pb(Mg_{1/3}Nb_{2/3})O_3$-$0.3PbTiO_3$ heterostructures. The electrically driven ferroelastic strain tunability of resistivity, with a giant gauge factor of 494, can be effectively modified by light stimulus. Moreover, the visible-light-excited photoresistivity response can be ferroelastically enhanced by up to 65%. This discovery illustrates the strong interplay between the ferroelastic-strain-induced and light-induced effects, mediated by lattice-charge-orbital coupling. Our work implies the potential application of correlated oxide-ferroelectric systems for future low-power high-density versatile electronic storage devices with light-sensing capability.

DOI: 10.1103/PhysRevApplied.17.014027

I. INTRODUCTION

Transition-metal oxides exhibiting strong electron correlation have stimulated broad interest for decades due to a wide range of fascinating phenomena, including high-temperature superconductivity, ferroelectricity, multiferroics, photovoltaic effects, planar Hall effects, colossal magnetoresistance effects, exchange bias, vertical hysteretic shifts, and Mott transitions, and promising applications in high-speed energy-efficient versatile electronic devices [1–8]. Among these correlated oxides, the perovskite vanadate of $LaVO_3$ (LVO) is a well-known prototypical Mott-Hubbard insulator with an electron configuration of $3d^2$ ($t_{2g}{}^2e_g{}^0$) that undergoes a magnetic phase transformation from paramagnetic to the antiferromagnetic (*C*-type spin ordering) state with concomitant *G*-type orbital ordering around $T_N \approx 140$ K [8]. Greatest emphasis has been placed on regulating the electronic and magnetic phases by exploiting diverse external parameters, such as temperature, current, an electric field, a stress field, and light irradiation, to pursue specific functional properties. For example, Tomimoto *et al.* [9] reported light-induced ultrafast melting of orbital ordering and a large reflectivity change of 15% in LVO single crystals using a Ti:sapphire regenerative amplifier system (photon energy of 1.55 eV), which is caused by the disordering of t_{2g} orbitals over 60 V sites per excitation photon. Choi and Sands [10] observed a ferroelectric field effect with an electrically tunable on:off resistance ratio of up to 2.5 in $LVO/(Ba,Sr)TiO_3/(Pb,La)(Zr,Ti)O_3/(La,Sr)CoO_3$ structures epitaxially grown on $SrTiO_3$ single-crystalline substrates, revealing the emergence of a depletion region (approximately 7 nm in depth). Razavi *et al.* [11] found current-induced suppression of the peak resistance or the change of multiple peaks to a plateau below 50 K for almost unstrained LVO films. Moreover, He *et al.* [12] identified metallic conductivity behavior for LVO films compressively strained on $SrTiO_3$ substrates; this is primarily attributed to polarity discontinuity at the interface but not lattice-induced electronic structure modification. Using density-functional-theory calculations, Sclauzero *et al.* [13] predicted that the compressive biaxial strain-induced increase in the hopping amplitude promoted the metallic state, while strain-induced crystal-field splitting always favored the insulating state. These two effects compete with each other and determine the final conductivity character. Apart from epitaxial strain, the growth mode [14], atomic displacements [15], oxygen content [16], and vanadium deficiency [17] also prove to play pivotal roles in the structural, electronic, and magnetic properties of LVO films. The challenge in elucidating pure or intrinsic strain effects is how to exclude the influence of these extrinsic ingredients on electronic and magnetic phases, namely, how to enable *in situ*, real-time, dynamic, and continuous control of lattice strain in thin films. The most common method is to utilize highly piezoelectrically active $Pb(Mg_{1/3}Nb_{2/3})O_3$-$PbTiO_3$ (PMN-PT) single crystals to impose electrically generated strain on the overlying functional films to modify their microstructures and related physical properties via interfacial elastic coupling [18,19]. Originally, the externally tunable strain and properties of the films can recover to the virgin states with

*zhengm@mail.ustc.edu.cn

the removal of the imposed electric field due to a linear piezo response of the PMN-PT substrate and is thus volatile [18,19], which is unfavorable for real device applications. Later, nonvolatile control is accessible at room temperature exclusively through non-180° ferroelastic polarization switching. Motivated by pioneering studies, a number of functional thin films, including luminescent $(Ba_{0.85}Ca_{0.15})_{0.998}Pr_{0.002}Ti_{0.9}Zr_{0.1}O_3$ [20], charge-ordered $Nd_{0.5}Sr_{0.5}MnO_3$ [21], ferromagnetic $Fe_{70}Rh_{30}$ [22], antiferromagnetic $Mn_{50}Pt_{50}$ [23], multiferroic $Bi_{0.95}Mn_{0.05}FeO_3$ [24], insulating V_2O_3 and $NdNiO_3$ [25,26], metallic $SrRuO_3$ and $LaNiO_3$ [27,28], and inducting Metglas [29], have been integrated onto the PMN-PT substrates and display strain-mediated nonvolatile switching of optical, magnetic, and electronic performances in a reversible way using the ferroelastic domain engineering technique. So far, the intrinsic effect of lattice strain on the nonvolatile electronic properties of LVO films has not been experimentally revealed. In spite of perpetual efforts dedicated to the single-stimulus-triggered modulation of the properties of LVO, multifield (e.g., optical and electrical) combined control of the electronic phase and related electronic transport have remained elusive, which would help explore the straintronic and optoelectronic physics of perovskite vanadates and assemble multifunctional memories and sensors with low power consumption and high speed.

Here, we epitaxially deposit Mott-insulating LVO thin films onto piezoelectric PMN-PT single-crystalline substrates and achieve reversible nonvolatile manipulation of multiple strain and resistivity states by changing the proportion of in-plane-polarization component relative to the out-of-plane counterpart of the substrate. Combining light stimulus with electrically assisted ferroelastic strain, we verify the strong coupling of the photoresistivity effect and electroresistivity response. This work indicates the possibility of photoresponsive correlated oxides for future high-density nonvolatile information-storage applications.

II. EXPERIMENTAL DETAILS

LVO thin films are grown on (111)-oriented one-side-polished single-crystalline substrates of PMN-PT by a pulsed-laser deposition system. The high-purity $LaVO_4$ ceramic target is ablated using a KrF (248 nm) excimer laser. The laser fluence and repetition rate are set at 1.5 J/cm^2 and 3 Hz, respectively. Film deposition is done at a constant substrate temperature of 720 °C with a base pressure below 10^{-6} Torr. The film thickness (100 nm) is monitored by the number of laser pulses. The silver films (120 nm thick) are fabricated on top of the LVO films and on the back of the PMN-PT substrates using thermal evaporation to form the top and bottom electrodes, respectively.

The crystallographic properties of the films are analyzed by a four-circle x-ray diffractometer (XRD, SmartLab, Rigaku Co., Japan) using Cu $K\alpha 1$ radiation with a Ni filter. The electrical transport properties of the structures are measured in the standard four-point configuration using a Keithley 2400 source meter. A continuous semiconductor laser diode with a wavelength of 532 nm and a fluence of 10 mW/cm^2 is utilized as the illumination source to irradiate the films. The gate electric field is supplied via electrical leads attached to the top and bottom Ag electrodes using a Keithley 6487 voltage source for switching the polarization vectors of the PMN-PT substrates. Figure 1(a) schematically illustrates the electrical measurement circuit of the LVO/PMN-PT structures under the coaction of the gate electric field and light illumination. Due to the much larger resistance ($10^9\,\Omega$) of the PMN-PT substrate than that (10^4–$10^5\,\Omega$) of the LVO film, the LVO film actually serves as the top electrode in the LVO/PMN-PT/Ag structure. Prior to any measurement, a large vertical bias field of $E = +8$ kV/cm (higher than the saturation field) is homogeneously loaded on the PMN-PT substrate for a period of time (30 min) and is then turned off, to introduce a single out-of-plane domain configuration [denoted as the $P_r^{\perp}$ state in Fig. 1(b)].

III. RESULTS AND DISCUSSION

Figure 1(d) depicts the XRD pattern of the LVO/PMN-PT system. Only the PMN-PT (*lll*) and LVO (*lll*) Bragg peaks are observed, implying that the LVO film is strongly (111)-oriented and single phase. The XRD ϕ scans reveal that the LVO film adopts the trifold symmetry of the PMN-PT (101) plane with the same azimuthal angles, a clear sign of heteroepitaxial growth of the LVO film on the PMN-PT substrate with perovskite structure. The initial vertical pseudocubic lattice spacing, d_{222} (approximately 1.128 Å), calculated from fitting of the LVO (222) Bragg peak is smaller than that of bulk LVO (approximately 1.133 Å) [30], suggesting that the LVO film is vertically compressively strained (−0.44%) on PMN-PT. Based on the Poisson relation, $\delta\varepsilon_{\perp} = -2\nu/(1-\nu)\delta\varepsilon_{\parallel}$ [31], and Poisson ratio, $\nu = 0.4$ [32], the lateral strain due to lattice misfit is estimated to be +0.33%, namely, the lattice expands in the (111) plane, which corresponds to the smaller lattice parameters of bulk LVO (3.925 Å) compared with those of PMN-PT (4.02 Å). The epitaxial heterointerface with good lattice matching is conducive for effective electric field tuning of the transport properties in PMN-PT-based systems that seek to adopt efficient interfacial elastic coupling.

The resistivity of the LVO film highly relies on the polarization domain configuration of the PMN-PT substrate. Figure 1(e) shows resistive switching in the LVO/PMN-PT structure under high- (bipolar) and low-amplitude (unipolar) gate electric fields using the measurement circuit in Fig. 1(a). Under high-amplitude bias-field

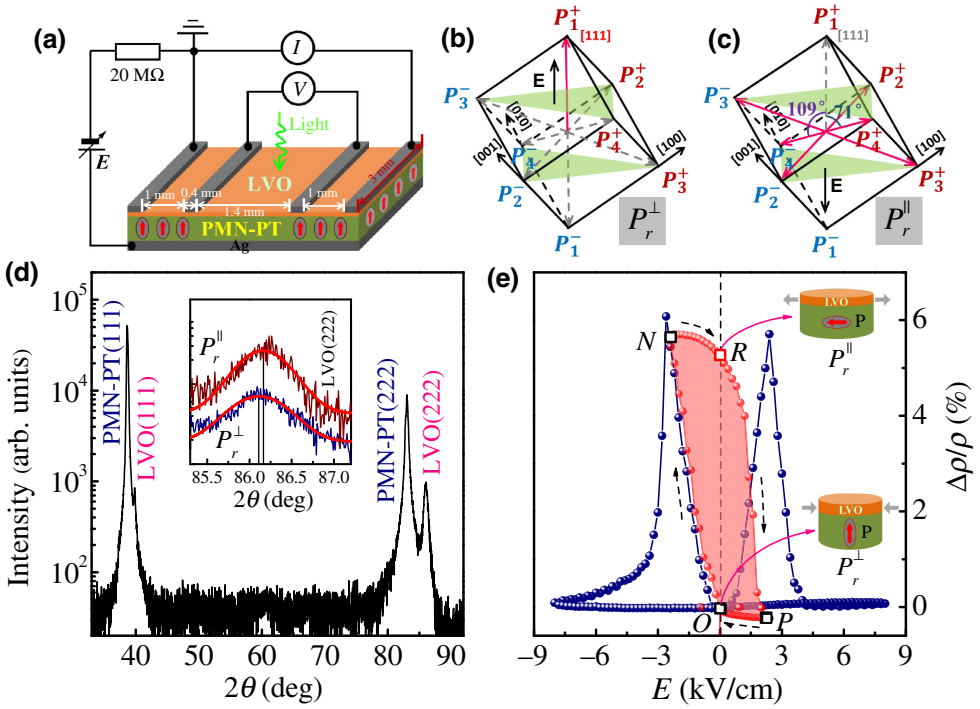

FIG. 1. (a) Schematic of electrical measurement geometry for the LVO/PMN-PT structure under an electric field and light illumination. Channel length and width of the prototype device are 1.4 and 3 mm, respectively, with silver electrodes of 0.4 mm wide. (b),(c) Polarization domain configurations of PMN-PT under $P_r^{\perp}$ and $P_r^{\parallel}$ states, respectively. (d) XRD pattern of the LVO/PMN-PT structure. Inset shows XRD patterns for the LVO (222) Bragg peak under $P_r^{\perp}$ and $P_r^{\parallel}$ states. (e) Resistive switching of the LVO/PMN-PT structure under the high- (bipolar) and low-amplitude (unipolar) gate electric fields at room temperature. Insets show in-plane and out-of-plane domain configurations.

sweeping, a typical symmetric butterflylike $\Delta\rho/\rho$ versus E curve (blue line) appears. Here, $\Delta\rho/\rho$ is defined as $\Delta\rho/\rho = [\rho(E) - \rho(P_r^{\perp})]/\rho(P_r^{\perp})$. We recall that the PMN-PT single crystals also show a well-defined butterflylike lateral strain versus electric field curve due to 180° polarization switching [20,24], which demonstrates that the lattice-strain effect is the primary driving force for resistivity variation of the LVO film. However, upon sweeping a low-amplitude bias field between $E = \pm 2.4$ kV/cm (close to but smaller than the coercive field, $E_{C(PMN-PT)}$, of PMN-PT), the hysteresislike $\Delta\rho/\rho$ versus E loop (peak line) is observed with two distinct resistivity states (O and R states) at zero bias, in analogy with reports on the V_2O_3/PMN-PT, $NdNiO_3$/PMN-PT, and $SrRuO_3$/PMN-PT systems [25–27]. This reversible and nonvolatile resistive change in the LVO film is crucially relevant to electrically generated ferroelastic strain owing to non-180° polarization switching in the substrates. In the PMN-PT single-crystalline substrate with a rhombohedral structure, the eight equivalent spontaneous polarization vectors in the virgin or unpoled states point in the body-diagonal directions with four equivalent structural domains (P_1, P_2, P_3, and P_4). After we impose a large vertical bias field of $E = +8$ kV/cm (higher than $E_{C(PMN-PT)}$) on the virgin PMN-PT substrate, a single out-of-plane polarization domain, P_1^{+}, is generated and aligned along the [111] direction (denoted as the $P_r^{\perp}$ state), as shown in Fig. 1(b). By exerting a

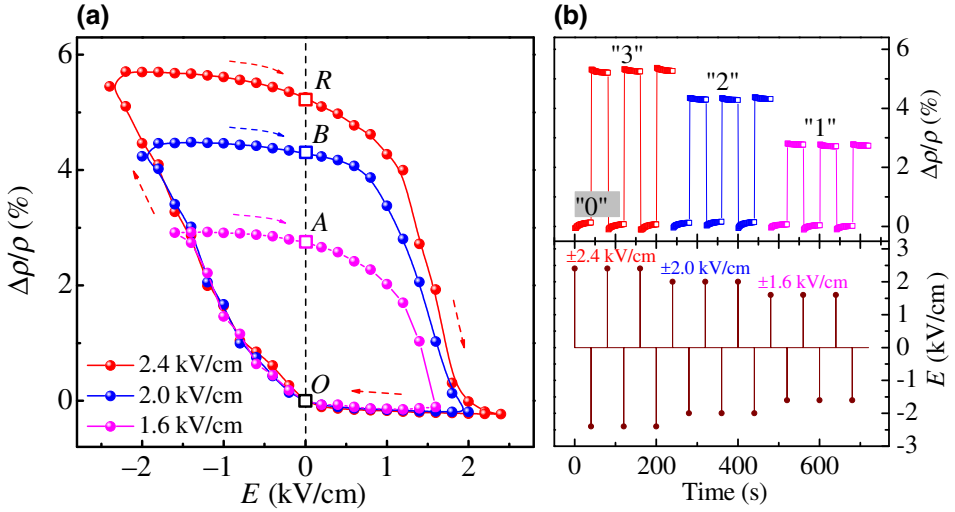

FIG. 2. (a) Unipolar resistive switching of the LVO/PMN-PT structure upon sweeping the gate bias fields with different amplitudes at room temperature. (b) Four nonvolatile and reversible resistivity states of the LVO film induced by imposing a stream of gate bias pulses with a width of 100 ms on the PMN-PT substrate.

subsequent small negative-bias field of $E = -2.4$ kV/cm on vertically poled PMN-PT and then removing it, the polarization vectors may rotate from P_1^+ to P_2^-, P_3^+, or P_4^- (109° ferroelastic switching) or from P_1^+ to P_2^+, P_3^-, or P_4^+ (71° ferroelastic switching), giving rise to a large in-plane-polarization component with multidomain configuration [denoted by $P_r^{\parallel}$ in Fig. 1(c)]. The occurrence of an in-plane-polarization domain triggered by non-180° domain switching is expected to generate lateral tensile strain in PMN-PT and can be transferred to the overlying LVO film [see inset of Fig. 1(e)], thereby increasing the film resistivity from the O to N states and then to the R state ($\Delta\rho/\rho = 5.26\%$). The electrically generated lateral tensile strain is manifested by the shift of the LVO (222) reflection peak to a higher Bragg angle in the inset of Fig. 1(d), which can be calculated to be $\delta\varepsilon_{\parallel} = +0.033\%$. Thus, the room-temperature gauge factor that characterizes the effectiveness of the strain tuning of resistivity, α [$\alpha = (\Delta\rho/\rho)/\delta\varepsilon_{\parallel}$], is 159, which is superior to the values for the $LaMnO_3$/PMN-PT (51.1) [33], $NdNiO_3$/PMN-PT (40.8) [26], and $SrRuO_3$/PMN-PT (3.9) [27] systems. Finally, after imposing another small positive-bias field of $E = +2.4$ kV/cm on laterally poled PMN-PT, the resistivity recovers to the original O state from the R state, since PMN-PT is switched back to the $P_r^{\perp}$ state and releases the previously generated lateral tensile strain. This result conspicuously establishes that ferroelastic strain emerges as an effective tool to realize nonvolatile resistive switching of epitaxial complex-oxide thin films by reversibly rotating the polarization vector between the vertical (single domain) and lateral (multidomain) directions in the PMN-PT substrate through simply changing the polarity of the gate bias near its coercive field. To enhance strain-mediated resistive switching, we can reduce the film thickness appropriately without lattice relaxation or use several buffer layers, e.g., $Ba_xSr_{1-x}TiO_3$, for coherent epitaxial growth of the LVO film with few defects at the interface, which can reinforce interfacial mechanical coupling and strain transfer from the substrate to the film.

The nonvolatile-resistivity state of the LVO/PMN-PT structure can be continuously manipulated between the O and R states by accurately adjusting the amplitude of the gate bias vertically imposed on the PMN-PT substrate, as shown in Fig. 2(a). Before each bias-cycling measurement, a reset step is required to set PMN-PT as the single out-of-plane-polarization domain state with the low-resistivity state (O state) by imposing appropriate positive-bias fields. Under the next application of negative-bias fields of $E = -2.4$, -2.0, and -1.6 kV/cm, the LVO film switches to different higher-resistivity states, i.e., R, B, and A states, respectively, which is closely related to the relative fraction of in-plane-polarization component and the resultant diverse stable residual lateral-strain states after non-180° domain switching [20,25,27]. Based on the nonvolatile ferroelastic strain effect, we demonstrate the feasibility of an electrically controlled low-power information-storage cell. As shown in Fig. 2(b), four resistivity states ("0" to "3" states) can be switched reversibly and are nonvolatile by imposing a stream of gate bias pulses on PMN-PT, which leads to the LVO/PMN-PT structure exhibiting an excellent nonvolatile-memory function. The writing operation is easy, fast, and energy efficient by applying a voltage pulse between the top and bottom electrodes. After applying a pulse of $E = +2.4$ kV/cm, the film resistance is measured for 40 s; then, another pulse of $E = -2.4$ kV/cm is applied to switch polarization from the out-of-plane direction to the in-plane direction and the resistance is measured for another 40 s. This process is repeated for three cycles. When we reduce the amplitude of the electric field from 2.4 kV/cm to 2.0 and 1.6 kV/cm, only a portion of out-of-plane ferroelectric domains are rotated into the in-plane direction and the induced in-plane strain decreases. The film resistance is then measured periodically by applying subsequent electric field pulses with amplitudes of 2.0 and 1.6 kV/cm. In this case, nonvolatile logic states are written in the form of remnant-strain states by applying pulse bias fields with amplitudes of $E = 2.4$, 2.0, and 1.6 kV/cm and a width of 100 ms in a high-speed and low-energy-consumption manner. Then, we can read out the same information from the corresponding remnant-resistance states (i.e., "0" state under $E = +2.4$, $+2.0$, and $+1.6$ kV/cm and "1," "2," and "3" states under $E = -2.4$, -2.0, and -1.6 kV/cm, respectively) in an easy and nondestructive way, which surpasses the sophisticated detection method of local magnetization in magnetic random access memory and the destructive reading operation of polarization in ferroelectric random access memory.

Figure 3(a) shows the photoresponses of the LVO films by switching the 532-nm laser on and off with an interval of 50 s at room temperature when the PMN-PT substrate is under the vertically ($P_r^{\perp}$) and laterally ($P_r^{\parallel}$) polarized states, respectively. The film resistivity is reduced moderately for both poled states when visible light is irradiated onto the LVO film, due to the generation of photocarriers [9]. It is noted that resistivity relaxation after photoexcitation is mainly the delocalization relaxation process of carriers, which may be related to the oxygen-dependent defects in the LVO films. Some carriers can be excited from the localized state due to oxygen-dependent defects into the conduction band [30]. However, such an excited electron state is unstable because some of the electrons tend to gradually move back to the positively charged oxygen-vacancy sites by Coulomb forces until an equilibrium is reached. Such an electron-delocalization process could result in resistance relaxation. Similar resistivity relaxation under light is also observed in other correlated oxide films, such as manganites [34]. Perturbation of the laser destroys the equilibrium of the physical degrees

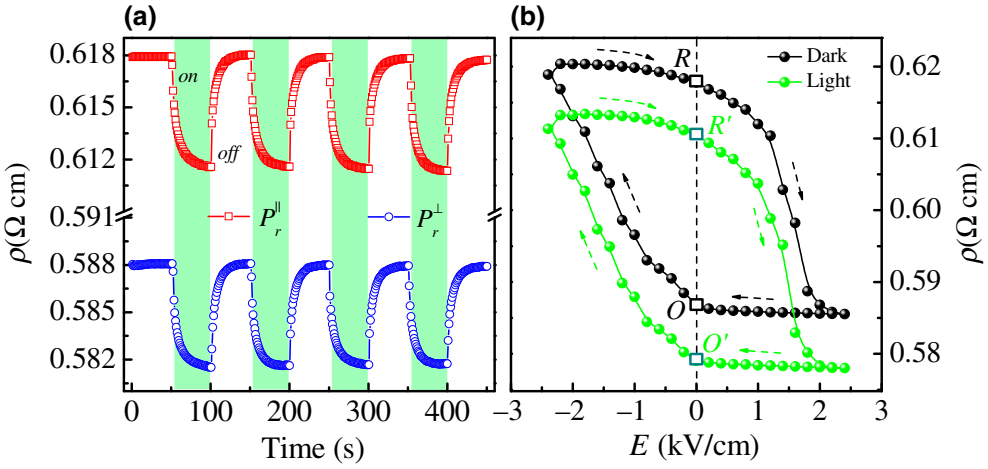

FIG. 3. (a) Resistive switching of the LVO film by turning on and off the 532-nm laser for the $P_r^{\perp}$ and $P_r^{\parallel}$ states at room temperature. (b) Unipolar resistivity hysteresis loops of the LVO/PMN-PT structure in the dark and under light illumination.

of freedom (such as charge and orbital) and induces the change in resistance. When the laser is turned off, the system returns to the original equilibrium state and relaxation is the process of recovery in the balanced physical degrees of freedom in correlated LVO films [34]. It is known that the heat effect is difficult to distinguish from the optical-electric effect under light illumination. In our experiments, two factors can be considered to neglect the heat effect. First, since the photon energy (2.33 eV) of the 532-nm laser used in the experiment is larger than the band gap of LVO (1.1 eV) [30], the light can be absorbed by the LVO films, and thus, the optical-electric effect is dominant. Second, the LVO/PMN-PT sample is attached to a copper cryostat using silver paint. If light illumination creates a little heat, the heat can also be dissipated into the holder, and the sample remains at a fixed temperature due to the closed-cycle cryostat. Therefore, the heating effect can be precluded. Upon switching the polarization from the $P_r^{\perp}$ state to the $P_r^{\parallel}$ state, the resistivity increases remarkably, irrespective of the presence or absence of light illumination. The ferroelastic-domain-switching-generated lateral tensile strain can reinforce crystal-field splitting between the t_{2g} orbitals and weaken the hopping amplitude through adjusting the octahedral tilt distortion, which favors the Mott-insulating state, and thus, raises the film resistivity [13]. To further unveil the coeffects of light irradiation and ferroelastic strain on electronic transport, we record the resistivity of the LVO films as a function of unipolar electric field in the dark and under illumination by a continuous laser at room temperature in Fig. 3(b). One can see that the resistive-switching hysteresis loops for these two irradiation conditions exhibit similar patterns, signaling that the ferroelastic-domain-switching dynamics is independent of photoexcitation. Obviously, the film resistivity under light illumination is visibly smaller than that in the dark for any fixed gate bias. Specifically, the *O* and *R* residual-resistivity states at zero bias in the dark shift down and transform into the corresponding *O'* and *R'* states, respectively, under light illumination, in conformity with the results in Fig. 3(a). Accordingly, four distinct residual-resistivity states can be generated under the combined application of light and gate-voltage pulses in LVO/PMN-PT structures. This finding means that the memory window of our prototype device can be manipulated by light illumination, which can be exploited in the design of high-density multifunctional storage devices with an extra capability to act as a light sensor.

Figure 4 depicts temperature-dependent electronic transport for the LVO film upon switching on and off laser illumination under the $P_r^{\perp}$ and $P_r^{\parallel}$ states, respectively. For the $P_r^{\perp}$ state in the dark, the film resistivity increases monotonously during the cooling process, which is an expected tendency due to the semiconducting behavior.

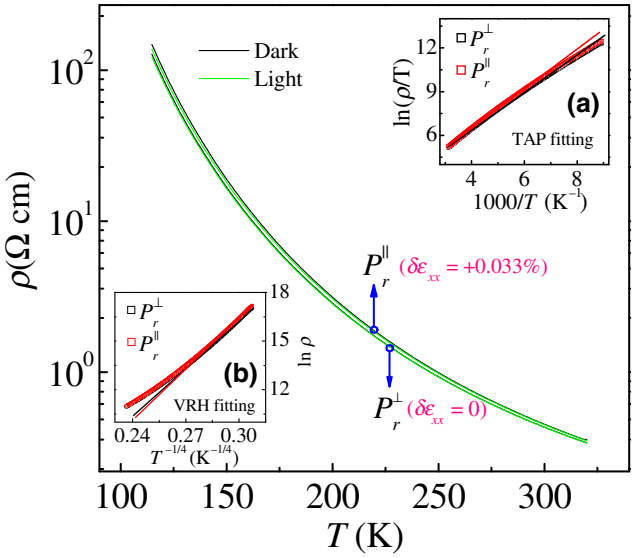

FIG. 4. Temperature dependence of resistivity for the LVO film upon switching on and off laser illumination for the $P_r^{\perp}$ and $P_r^{\parallel}$ states, respectively. Insets (a),(b) show $\ln(\rho/T)$ versus $1000/T$ and $\ln\rho$ versus $T^{-1/4}$ curves for the $P_r^{\perp}$ and $P_r^{\parallel}$ states, respectively.

Accompanied by polarization rotated from the $P_r^{\perp}$ state to the $P_r^{\parallel}$ state, the electrically induced lateral tensile strain ($\delta\varepsilon_{\parallel} = +0.033\%$) leads to an enhancement in resistivity throughout the entire temperature range. At high temperatures ($T > T_N$), for both poled states, resistivity data can be well fitted by the equation $\rho = \rho_0 \mathrm{T}\, exp(E_a/k_B \mathrm{T})$, where k_B is the Boltzmann constant and E_a is the activation energy [35]. This result provides evidence for a thermally activated polaron-hopping (TAP) model as the conduction mechanism for electronic transport at $T > T_N$. Here, E_a can be derived from linear fitting of the $\ln(\rho/T)$ versus $1000/T$ curve [see inset (a) of Fig. 4]. Upon poling from the $P_r^{\perp}$ state to the $P_r^{\parallel}$ state, the E_a value is found to increase from 0.108 to 0.112, implying enhanced localization of carriers due to lateral lattice expansion. Meanwhile, both E_a values are much smaller than the band gap (1.1 eV), which is usually ascribed to the excitation of carriers from the localized state, due to oxygen-dependent defects, into the conduction band [30]. At low temperatures ($T < T_N$), electronic transport can be described via a three-dimensional variable-range-hopping (VRH) model with $\rho = \rho_0 [exp(\mathrm{T}_0/\mathrm{T})^{1/4}]$ [36], as corroborated by the linear response of $\ln\rho$ to $T^{-1/4}$ [see inset (b) of Fig. 4]. This conduction mechanism discloses the occurrence of strong localized states near the Fermi level in the LVO films due to charge-orbital ordering. Aside from electrically generated transport variation, the LVO film also shows a noticeable drop in resistivity upon light illumination over the whole temperature region, regardless of whether it is in the $P_r^{\perp}$ state or the $P_r^{\parallel}$ state, which is caused by the generation and excitation of photocarriers and melting of orbital ordering [9]. Our work demonstrates the effective manipulation of lattice and charge degrees of freedom and related electrical properties in complex-oxide heterostructures via combined electrical and light stimuli.

Since electrically controlled ferroelastic strain and light can both strongly alter electronic transport in LVO/PMN-PT structures, it is inferred that the electroresistivity effect (i.e., ferroelastic strain effect) and photoinduced effect may couple with each other. Figure 5(a) shows the ferroelastic strain tunability of resistivity ($\Delta\rho/\rho$) versus temperature in the dark and under light illumination. Here, $\Delta\rho/\rho$ is defined as $\Delta\rho/\rho = [\rho(P_r^{\parallel}) - \rho(P_r^{\perp})]/\rho(P_r^{\perp})$. In the dark, $\Delta\rho/\rho$ rises upon cooling and attains a maximum value of 16.3% at $T = 115$ K, implying that the charge-orbital ordered phase in the LVO film is rather susceptible to the ferroelastic-domain-switching-generated lateral tensile strain at low temperature. Notably, $\Delta\rho/\rho$ is reduced hugely upon light illumination, especially in the low-temperature region. For example, $\Delta\rho/\rho$ at $T = 115$ K decreases from 16.3% in the dark to 12.9% under light illumination, a reduction of 20.8%. Similar optical control of the strain tunability of resistance is also observed in other correlated oxide (e.g., $SrRuO_3$)-PMN-PT systems [37]. The application of light would engender more carriers with enhanced hopping and melting of orbital ordering in the LVO films, which disfavors the Mott-insulating state, and thus, suppresses strain-induced tuning of the electronic transport properties in the LVO/PMN-PT structures. To quantify the effect of ferroelastic strain on electronic transport, the gauge factor, α, which characterizes the sensitivity of the resistivity to ferroelastic strain, is plotted as a function of temperature in the dark and under light illumination in the inset of Fig. 5(a). Notably, ferroelastic strain is almost independent of temperature, and thus, its disparity can be neglected here. α increases upon cooling with or without the application of light. Maximal α values of 494 and 393 are achieved at $T = 115$ K in the dark and under light illumination, respectively, which indicates that a change of lateral tensile strain by 0.033% leads to a maximal relative variation of resistivity by 16.3% and 12.9% for the LVO films at $T = 115$ K. The optically induced reduction of the gauge factor further reveals that light suppresses the ferroelastic strain effect in LVO/PMN-PT heterostructures. Besides the optically tunable electroresistivity effect, the coupling of photoinduced and strain-induced effects can also be manifested by a ferroelastically tunable photoresistivity response. Figure 5(b)

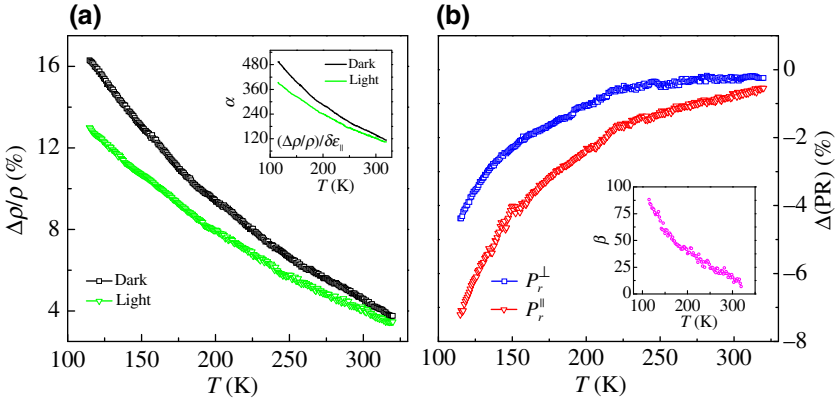

FIG. 5. (a) Temperature dependence of ferroelastic strain tunability of resistivity ($\Delta\rho/\rho$) for the LVO/PMN-PT structure in the dark and under light illumination. Inset shows gauge factor α as a function of temperature in the dark and under light illumination. (b) Temperature dependence of photoresistivity [Δ(PR)] for the LVO/PMN-PT structure for the $P_r^{\perp}$ and $P_r^{\parallel}$ states, respectively. Inset shows the figure of merit, β, as a function of temperature.

shows the photoinduced relative-resistivity change [i.e., $\Delta(\mathrm{PR})$] of the LVO film under the $P_r^{\perp}$ and $P_r^{\parallel}$ states, respectively. Here, $\Delta(\mathrm{PR})$ is defined as $\Delta(\mathrm{PR}) = (\rho_{light} - \rho_{dark})/\rho_{\mathrm{dark}}$. For both of the poled states, the $\Delta(\mathrm{PR})$ is enhanced in magnitude with decreasing temperature. After switching the polarization from the $P_r^{\perp}$ state to the $P_r^{\parallel}$ state, the magnitude of $\Delta(\mathrm{PR})$ increases dramatically, particularly below T_N. For example, the $|\Delta(\mathrm{PR})|$ value at $T = 115$ K is enlarged from 4.37% for the $P_r^{\perp}$ state to 7.21% for the $P_r^{\parallel}$ state, an enhancement of 65%. Such a ferroelastically reinforced photoresistivity effect could be ascribed to the lateral-tensile-strain-generated localization of charge carriers, which increases the effective number of electrons that can be excited to the conduction band. The figure of merit that evaluates the effectiveness of the ferroelastic strain tunability of photoresistivity, β [$\beta = |\Delta(\mathrm{PR})_{\parallel}\text{-}\Delta(\mathrm{PR})_{\perp}|/\delta\varepsilon_{\parallel}$], rises gradually as the temperature decreases and reaches an ultimate value of 86 at $T = 115$ K [see inset of Fig. 5(b)], signaling the sharp response of the photoresistivity effect to ferroelastic strain at low temperature. This result suggests that an evolution of lateral tensile strain by 0.033% causes the largest variation in photoresistivity of 2.84% for the LVO film at $T = 115$ K. These data together prove the mutual interaction between the ferroelastically generated and optically generated effects, which further confirm that the lattice and charge degrees of freedom are strongly correlated with each other in LVO/PMN-PT heterostructures.

IV. CONCLUSIONS

We report the electrically triggered nonvolatile control of electronic transport in LVO/PMN-PT structures. Four well-distinguished resistivity states can be converted in a reversible and nonvolatile way by accurately adjusting the amplitude of the gate bias pulse vertically imposed on the PMN-PT substrate, which is associated with the relative fraction of in-plane-polarization component and the resulting dissimilar residual lateral-strain states after non-180° ferroelastic domain switching. In particular, we find that the ferroelastic strain tunability of resistivity is optically controllable. Moreover, the photoresistivity response can be reinforced by 65% through electrically generated ferroelastic strain. These findings demonstrate that the light-generated and ferroelastic-strain-generated effects couple with each other, arising from the intimate correlation between charge and lattice degrees of freedom. Our work is instructive for achieving ferroelastically and optically combined control of the physical properties of hybrid Mott-oxide–ferroelectric systems, which enables practical implementations of energy-efficient high-density nonvolatile multifunctional memory devices with an additional functionality (e.g., light sensor).

ACKNOWLEDGMENTS

This work is supported by the National Natural Science Foundation of China (Grant No. 12004423), the Natural Science Foundation of Jiangsu Province (Grant No. BK20200662), the Program for High-Level Entrepreneurial and Innovative Talents Introduction of Jiangsu Province, and the Open Sharing Fund for the Large-Scale Instruments and Equipments of China University of Mining and Technology (CUMT) (Grant No. DYGX-2021-019).

[1] P. A. Lee, N. Nagaosa, and X.-G. Wen, Doping a Mott insulator: Physics of high-temperature superconductivity, Rev. Mod. Phys. **78**, 17 (2006).

[2] M. Uehara, S. Mori, C. H. Chen, and S.-W. Cheong, Percolative phase separation underlies colossal magnetoresistance in mixed-valent manganites, Nature **399**, 560 (1999).

[3] H. Bai, J. Li, Y. Hong, and Z. Zhou, Enhanced ferroelectricity and magnetism of quenched $(1-x)BiFeO_3$-$xBaTiO_3$ ceramics, J. Adv. Ceram. **9**, 511 (2020).

[4] S. Cheng, Z. Fan, L. Zhao, H. Guo, D. Zheng, Z. Chen, M. Guo, Y. Jiang, S. Wu, Z. Zhang, J. Gao, X. Lu, G. Zhou, X. Gao, and J.-M. Liu, Enhanced photovoltaic efficiency and persisted photoresponse switchability in $LaVO_3/Pb(Zr_{0.2}Ti_{0.8})O_3$ perovskite heterostructures, J. Mater. Chem. C **7**, 12482 (2019).

[5] R. Tomar, S. Kakkar, C. Bera, and S. Chakraverty, Anisotropic magnetoresistance and planar Hall effect in (001) and (111) $LaVO_3/SrTiO_3$ heterostructures, Phys. Rev. B **103**, 115407 (2021).

[6] C. Jin, Y. Zhu, W. Han, Q. Liu, S. Hu, Y. Ji, Z. Xu, S. Hu, M. Ye, and L. Chen, Exchange bias in flexible freestanding $La_{0.7}Sr_{0.3}MnO_3/BiFeO_3$ membranes, Appl. Phys. Lett. **117**, 252902 (2020).

[7] M. Zheng, X. Li, W. Xiao, W. Wang, and H. Ni, Oxygen deficiency and cooling field driven vertical hysteretic shift in epitaxial $SrRuO_3/SrTiO_3$ heterostructures, Appl. Phys. Lett. **111**, 152405 (2017).

[8] M. Stübinger, J. Gabel, P. Scheiderer, M. Zapf, M. Schmitt, P. Schütz, B. Leikert, J. Küspert, M. Kamp, P. K. Thakur, T.-L. Lee, P. Potapov, A. Lubk, B. Büchner, M. Sing, and R. Claessen, Hard x-ray photoemission spectroscopy of $LaVO_3/SrTiO_3$: Band alignment and electronic reconstruction, Phys. Rev. B **103**, 235128 (2021).

[9] S. Tomimoto, S. Miyasaka, T. Ogasawara, H. Okamoto, and Y. Tokura, Ultrafast photoinduced melting of orbital order in $LaVO_3$, Phys. Rev. B **68**, 035106 (2003).

[10] W. Choi and T. Sands, Ferroelectric field effect in epitaxial $LaVO_3/(Ba,Sr)TiO_3/(Pb,La)(Zr,Ti)O_3/(La,Sr)CoO_3$ heterostructures, J. Appl. Phys. **93**, 4761 (2003).

[11] F. S. Razavi, S. Jamali Gharetape, D. A. Crandles, G. Christiani, R. K. Kremer, and H.-U. Habermeier, Evidence for random networks of diodes in thin films of $LaVO_3$ on $SrTiO_3$ substrates, Appl. Phys. Lett. **96**, 042110 (2010).

[12] C. He, T. D. Sanders, M. T. Gray, F. J. Wong, V. V. Mehta, and Y. Suzuki, Metal-insulator transitions in

epitaxial $LaVO_3$ and $LaTiO_3$ films, Phys. Rev. B **86**, 081401(R) (2012).
[13] G. Sclauzero, K. Dymkowski, and C. Ederer, Tuning the metal-insulator transition in d^1 and d^2 perovskites by epitaxial strain: A first-principles-based study, Phys. Rev. B **94**, 245109 (2016).
[14] H. Zhang, L. R. Dedon, L. W. Martin, and R. Engel-Herbert, Self-regulated growth of $LaVO_3$ thin films by hybrid molecular beam epitaxy, Appl. Phys. Lett. **106**, 233102 (2015).
[15] G. Masset, O. Copie, J. Ghanbaja, K. Dumesnil, L. Pasquier, D. Pierre, and S. Andrieu, Epitaxial growth and structure of $LaVO_3$ and $PrVO_3$ thin films, Phys. Rev. Mater. **4**, 064417 (2020).
[16] Y. Hotta, Y. Mukunoki, T. Susaki, H. Y. Hwang, L. Fitting, and D. A. Muller, Growth and epitaxial structure of $LaVO_x$ films, Appl. Phys. Lett. **89**, 031918 (2006).
[17] S. J. Gharetape, M. P. Singh, F. S. Razavi, D. A. Crandles, L. Y. Zhao, and K. T. Leung, Effect of vanadium deficiency on properties of polycrystalline $LaVO_3$, Appl. Phys. Lett. **98**, 052509 (2011).
[18] R. K. Zheng, Y. Jiang, Y. Wang, H. L. W. Chan, C. L. Choy, and H. S. Luo, Ferroelectric poling and converse-piezoelectric-effect-induced strain effects in $La_{0.7}Ba_{0.3}MnO_3$ thin films grown on ferroelectric single-crystal substrates, Phys. Rev. B **79**, 174420 (2009).
[19] M. Zheng, M. M. Yang, Q. X. Zhu, X. Y. Li, G. Y. Gao, R. K. Zheng, Y. Wang, X. M. Li, X. Shi, H. S. Luo, and X. G. Li, Tunable interface strain coupling and its impact on the electronic transport and magnetic properties of $La_{0.5}Ca_{0.5}MnO_3/Pb(In_{1/2}Nb_{1/2})O_3 - Pb(Mg_{1/3}Nb_{2/3})O_3 - PbTiO_3$ multiferroic heterostructures, Phys. Rev. B **90**, 224420 (2014).
[20] M. Zheng, H. L. Sun, M. K. Chan, and K. W. Kwok, Reversible and nonvolatile tuning of photoluminescence response by electric field for reconfigurable luminescent memory devices, Nano Energy **55**, 22 (2019).
[21] M. Zheng, X. K. Xu, H. Ni, Y. P. Qi, X. M. Li, and J. Gao, Ferroelastically and magnetically co-coupled resistive switching in $Nd_{0.5}Sr_{0.5}MnO_3$/PMN-PT(011) multiferroic heterostructures, Appl. Phys. Lett. **112**, 123502 (2018).
[22] M. Zheng, T. Usami, and T. Taniyama, Shear-strain-mediated large nonvolatile tuning of ferromagnetic resonance by an electric field in multiferroic heterostructures, NPG Asia Mater. **13**, 7 (2021).
[23] H. Yan, *et al.*, A piezoelectric, strain-controlled antiferromagnetic memory insensitive to magnetic fields, Nat. Nanotechnol. **14**, 131 (2019).
[24] M. M. Yang, X. Q. Zhao, J. Wang, Q. X. Zhu, J. X. Zhang, X. M. Li, H. S. Luo, X. G. Li, and R. K. Zheng, Intrinsic and quantitative effects of in-plane strain on ferroelectric properties of Mn-doped $BiFeO_3$ epitaxial films by in situ inducing strain in substrates, Appl. Phys. Lett. **104**, 052902 (2014).
[25] P. Salev, J. del Valle, Y. Kalcheim, and I. K. Schuller, Giant nonvolatile resistive switching in a mott oxide and ferroelectric hybrid, Proc. Natl. Acad. Sci. **116**, 8798 (2019).
[26] J. Yan, M. Xu, T. Chen, M. Yang, F. Liu, H. Wang, L. Guo, Z. Xu, F. Fan, G. Gao, S. Dong, X. Li, H. Luo, W. Zhao, and R. K. Zheng, Manipulation of the Electronic Transport Properties of Charge-Transfer Oxide Thin Films of $NdNiO_3$ Using Static and Electric-Field-Controllable Dynamic Lattice Strain, Phys. Rev. Appl. **11**, 034037 (2019).
[27] M. Zheng, H. Ni, Y. P. Qi, W. Y. Huang, J. L. Zeng, and J. Gao, Ferroelastic strain control of multiple nonvolatile resistance tuning in $SrRuO_3$/PMN-PT(111) multiferroic heterostructures, Appl. Phys. Lett. **110**, 182403 (2017).
[28] M. Li, Z. Gao, X. Wang, C. Kang, X. Liu, C. Jia, C. Luo, and W. Zhang, Non-volatile resistance switching in $LaNiO_3$ films on PMN-PT substrates, J. Phys. D: Appl. Phys. **53**, 325306 (2020).
[29] B. Peng, C. Zhang, Y. Yan, and M. Liu, Voltage-Impulse-Induced Nonvolatile Control of Inductance in Tunable Magnetoelectric Inductors, Phys. Rev. Appl. **7**, 044015 (2017).
[30] L. Wang, Y. Li, A. Bera, C. Ma, F. Jin, K. Yuan, W. Yin, A. David, W. Chen, W. Wu, W. Prellier, S. Wei, and T. Wu, Device Performance of the Mott Insulator $LaVO_3$ as a Photovoltaic Material, Phys. Rev. Appl. **3**, 064015 (2015).
[31] S. P. Timoshenko and J. N. Goodier, *Theory of Elasticity* (McGraw-Hill, New York, 1987), Chap. 2.
[32] H. Rotella, U. Lüders, P.-E. Janolin, V. H. Dao, D. Chateigner, R. Feyerherm, E. Dudzik, and W. Prellier, Octahedral tilting in strained $LaVO_3$ thin films, Phys. Rev. B **85**, 184101 (2012).
[33] R. K. Zheng, Y. Wang, H.-U. Habermeier, H. L. W. Chan, X. M. Li, and H. S. Luo, Interface strain coupling and its impact on the transport and magnetic properties of $LaMnO_3$ thin films grown on ferroelectrically active substrates, J. Alloys Compd. **519**, 77 (2012).
[34] S. G. Zhao, K. X. Jin, and C. L. Chen, Photoinduced effect in charge-ordering $La_{0.5}Ca_{0.5}MnO_3$ film, J. Appl. Phys. **101**, 083701 (2007).
[35] G. J. Snyder, R. Hiskes, S. DiCarolis, M. R. Beasley, and T. H. Geballe, Intrinsic electrical transport and magnetic properties of $La_{0.67}Ca_{0.33}MnO_3$ and $La_{0.67}Sr_{0.33}MnO_3$ MOCVD thin films and bulk material, Phys. Rev. B **53**, 14434 (1996).
[36] K. Maiti, N. Y. Vasanthacharya, and D. D. Sarma, Doping dependence of transport and magnetic properties in La1_xCaxVO3, J. Phys.: Condens. Matter **9**, 7507 (1997).
[37] M. Zheng, H. Ni, W. Y. Huang, Y. P. Qi, J. L. Zeng, and J. Gao, Optically and electrically co-controlled resistance switching in complex oxide heterostructures, Appl. Phys. Lett. **111**, 172901 (2017).

Correction: The math terms in the HTML version were processed incorrectly in the production process and have been rendered properly now.